From disorder to order: a dynamic approach to mesophase formation in soft sphere model

María Victoria Uranga Wassermann, ¹ Ezequiel R. Soulé, ¹ and Cristian Balbuena^{1, a)}
Institute of Materials Science and Technology (INTEMA), University of Mar del Plata and National Research Council (CONICET), Colón 10850, 7600 Mar del Plata, Argentina.

(Dated: 29 August 2024)

This study explores the dynamics of self-assembly and mesophase formation through molecular dynamics simulations of hexagonal and lamellar systems using a simplified coarse-grained model. We focus on characterizing the order-disorder transitions driven by temperature variations and emphasize the often overlooked disordered regime, which serves as a precursor to periodic mesoscale ordering. Our findings not only underscore the morphological richness of the disordered regime, comparable to that of its periodic counterparts, but also reveal the presence of clustering regimes within isotropic phases, thus corroborating prior experimental and theoretical observations. By employing the dynamic correlation coefficient, this work introduces a novel approach to understanding the fundamental mechanisms of mesophase formation, providing new insights into the complex dynamics of self-assembly.

I. INTRODUCTION

Materials capable of self-assembly play a crucial role in advancing technology by harnessing molecules' natural tendency to arrange themselves. A key focus is on mesophases, which act as bridges between the disorder of liquids and the ordered nature of crystalline solids. These intermediate states enable the discovery of materials with exceptional properties, applicable in fields such as engineering for unique optical traits and innovations in drug delivery^{1,2}. The focus on materials that spontaneously organize or demonstrate microphase separation has intensified, highlighting their capacity to modulate macroscopic features through microstructural control. This transition from disorder to order manifests in the creation of mesophases with dimensional variabilities from the nanometer to the micrometer scale. Amphiphilic molecules and block copolymers are noteworthy examples of this self-organizing phenomenon, driven by the diverse physicochemical interactions among their segments, leading to a plethora of structural formations. Tailoring these formations allows for the customization of materials for specific needs based on their self-assembled configurations and domain dimensions $^{3-5}$.

Understanding the complexities of self-assembly and mesophase formation is essential for the development of tailor-made materials with specific functionalities 6 . Understanding how molecules organize themselves at the molecular level facilitates the design of materials for particular applications. Control of mesophase formation through self-assembly is achieved by an exhaustive exploration of microscopic mechanisms $^{7-10}$.

Research in this field has taken a dual approach, merging experimental studies with theoretical models. In general, experimental studies provide direct insights into

structural configurations and transitions between different phases $^{4,11-14}$, while theoretical studies offer a framework for understanding the mechanisms at play $^{15-24}$.

The ordered phase is notably well-described and characterized in both experimental and modeling efforts, highlighting its structural and transitional properties. However, our understanding of the disordered microphase regime remains relatively underdeveloped. Disordered micellar or clustering regimes within isotropic phases have been identified, suggesting a level of order that prevails even without a well-defined structured framework, particularly in systems with shortrange attractive and long-range repulsive interactions $(SALR)^{25-30}$. Moreover, one-dimensional systems with exact solutions also exhibit clustering transitions, providing further evidence that clustering is a pervasive feature across different scales and types of systems³¹. Mean-field and density functional theories may account for the structural heterogeneity inherent to this regime, but they require previous knowledge of the possible structures. Existing liquid state theories also struggle to capture its rich morphological features.

Molecular dynamics simulations have become increasingly important in this field, offering deep insights into the structure and dynamics of self-assembly processes. These simulations are essential for understanding the details of both ordered and disordered phases, allowing researchers to explore how various parameters affect mesophase formation^{22–24,30,32}. Despite extensive studies using model microphase formers, only a few have utilized accurate equilibrium phase data, highlighting an area for potential improvement in future research. Recently, the KM model²³, known for simulating block copolymer-like phases, has been instrumental in observing these transitions. For example, this model has been effectively employed to delve into the characteristics of lamellar, cylindrical, and gyroid phases^{33–36}.

In our work, we employ a dynamic characterization approach, leveraging molecular dynamics simulations to

^{a)}Electronic mail: cbalbuena@fi.mdp.edu.ar

units.

probe into the complexities of mesophase formation. We explore correlated particle movements, string roles, and Pearson correlation coefficients, introducing a novel perspective on the dynamics of mesophases in the KM model. This approach not only deepens our understanding of mesophase behavior but also highlights the critical impact of dynamic correlations on their formation, providing new insights that could guide the design of advanced materials.

II. METHODS

This study utilizes a soft-sphere model comprising two distinct particle types (A and B), following the approach outlined by Kumar and Molinero²³. Interactions between particles are described using an isotropic Stillinger-Weber potential, given by:

$$U(r_{ij}) = A\epsilon \left[B \left(\frac{\sigma}{r_{ij}} \right)^p - 1 \right] \exp \left(\frac{\sigma}{r_{ij} - a\sigma} \right), \quad (1)$$

where ϵ and σ represent the interaction strength and particle size, respectively, and r_{ij} is the distance between particles i and j. The parameters used are A=7.0496, B=0.6022, p=4, and $a=1.80^{23}$. With these parameters, the potentials have minima at 1.112σ and vanish at 1.8σ . All quantities are expressed in reduced units, where the energy scale ϵ and the size parameter σ define the units as follows: temperature is expressed as $\frac{\epsilon}{k_B}$ and time is measured in units of $\sqrt{\frac{m\sigma^2}{\epsilon}}$. Except the potential well depth, all other quantities are reported in reduced

Mesophase formation, similar to that in block copolymers, is influenced by the values of ϵ and σ , and the system composition, represented by the fraction of type B particles X_B , defined as the ratio of type B particles to the total number of particles. Previous studies have shown that mesophase formation occurs when the attraction between different particle types is greater than that between similar particles ($\epsilon_{AB}/\epsilon_{BB} > 1$), and when particles of different types cannot approach each other as closely as those of the same type $(\sigma_{AB}/\sigma_{BB} > 1)^{23}$. The variations in particle type fractions and this packing asymmetry lead to the formation of various block-copolymer-like mesophases.

This study focuses on two specific mesophases: a lamellar system with $X_B = 0.5$ and $\epsilon_{AB} = 1.4\,\mathrm{kcal\ mol^{-1}}$, and a hexagonal system with $X_B = 0.24$ and $\epsilon_{AB} = 2.0\,\mathrm{kcal\ mol^{-1}}$. For both setups, the parameters $\sigma_{AA} = \sigma_{BB} = 1$, $\epsilon_{AA} = \epsilon_{BB} = 1.0$, and $\sigma_{BA} = 1.15$ were selected, based on the phase diagram by Kumar and Molinero²³. These parameters ensure stable lamellar and hexagonal mesophases at specific temperatures.

Molecular dynamics (MD) simulations were performed using the LAMMPS software³⁷. Two system sizes were examined: a smaller system with 3594 particles for the

lamellar system and 4096 particles for the hexagonal system, and a larger system with 28752 particles for both configurations to improve statistical accuracy. To obtain initial equilibrated configurations at the highest temperatures, particles were randomly positioned in the simulation box and velocities were assigned following a Boltzmann distribution. Initial simulations employed an NPT ensemble at a pressure of P=1 for 10^5 timesteps, followed by 10⁵ timesteps in NVT and NVE ensembles. A final equilibration run of 10⁶ timesteps in the NPT ensemble ensured that energy and volume remained stable. Using these configurations, trajectories at lower temperatures were generated by starting from the equilibrated state of the nearest higher temperature and following the same equilibration protocol. Subsequent simulations to generate equilibrated trajectories for the binary particle system were conducted in an NPT ensemble for 10⁶ timesteps, with periodic boundary conditions in all directions. Temperature and pressure were controlled using the Nose-Hoover thermostat and barostat, and force integration was carried out using the velocity Verlet algorithm with a timestep of $\Delta t = 0.005$. The systems were analyzed through equilibrated trajectories over a temperature range from 1.8 down to 0.3, in decrements of 0.1.

III. RESULTS AND DISCUSSION

In this study, we characterized phase transitions in both systems by measuring the average volume at different temperatures. Equilibrated trajectories were generated at various temperatures while maintaining constant pressure, allowing the system's volume to fluctuate. The observed volume behavior is illustrated in Figure 1. The significant change in volume during the phase transition from order to disorder is notable, enabling us to determine the critical temperatures, T_{OD} , for both the hexagonal and lamellar systems. In both cases, T_{OD} is found to occur in the vicinity of T = 1.0, specifically around T = 0.95 for the lamellar system, and slightly higher at T=1.05 for the hexagonal system. This particularity of the KM model does not align with what is typically expected in block copolymer systems and existing theoretical frameworks, where the transition to the lamellar phase is generally considered to be a weakly firstorder transition, often without the pronounced jump observed in our results. For instance, studies by Bates and Fredrickson⁴ have shown that the transition to the lamellar phase in block copolymers is usually characterized by a gradual change in thermodynamic quantities, unlike the abrupt transition evidenced in this model. This discrepancy suggests that the interaction parameters and specific conditions within the KM model may lead to a more pronounced first-order transition, differing from the weaker transitions observed in experimental systems.

The transition that the system undergoes at T_{OD} has been characterized by employing various types of struc-

tural parameters, which allowed for a deeper understanding of the mechanisms underlying transitions from disordered to ordered states^{34,36,38,39}. However, an interesting result is the apparent change in the volume behavior above the T_{OD} temperature, specifically in the isotropic region, where a change of slope and curvature is identified at a temperature defined as T_x . In the range $T_{OD} < T < T_x$, a linear increase of volume with temperature is observed, while for temperatures above T_x , the rate of volume change accelerates, indicating an increase in the thermal expansion coefficient. In our previous research, we have observed structural changes around this temperature; specifically, below T_x , the system exhibits a tendency for particles of the same type to cluster together, locally resembling the structure of the ordered phase³⁹. Note that this transformation is not a phase transition, because it involves only a finite number of particles and T_x is, probably, not precisely defined. Most likely, the tendency to cluster gradually diminishes as T increases and T_x represents the temperature at which clustering ceases to have a noticeable effect, akin to the concept of "critical micellar temperature" observed in surfactant and copolymer systems. This insight adds to our understanding of the complex dynamics during the system's transition phases, highlighting the presence of behaviors not previously documented in this model.

Additionally, similar findings have been reported in studies of systems with SALR interactions, where the formation of clusters leads to significant changes in the pressure-density relationship. These results are indicative of a broader phenomenon where clustering impacts the thermodynamic properties of the system. For instance, Santos et al. observed a change in the slope of the pressure versus density curve under certain conditions, attributed to the onset of cluster formation⁴⁰. This behavior mirrors our observations at T_x , where the formation of clusters corresponds to marked volumetric changes. Furthermore, Charbonneau et al. have structurally and dynamically characterized the different density-dependent regimes in a SALR model, elucidating the complex interplay between clustering and the system's relaxation dynamics³⁰. In our case, it is expected that the emergence of clustering or micellization is influenced by the system's pressure. Due to the nature of the interaction potential, increasing pressure promotes the aggregation of particles of the same type, as this reduces the overall volume. Therefore, higher pressures are likely to favor the clustering regime in our model.

An qualitative way to illustrate the structural changes that occur around T_x is through the visualization of molecular dynamics configurations of the system at three different temperatures, which represent different thermal regions: $T_1 < T_{OD} < T_2 < T_x < T_3$. In Figure 2, the hexagonal system at these specific temperatures is displayed, where spheres represent the majority particles and isosurfaces represent the minority particles. Qualitatively, it is appreciated that, above T_x , particles lack a defined structural connection. However, for tempera-

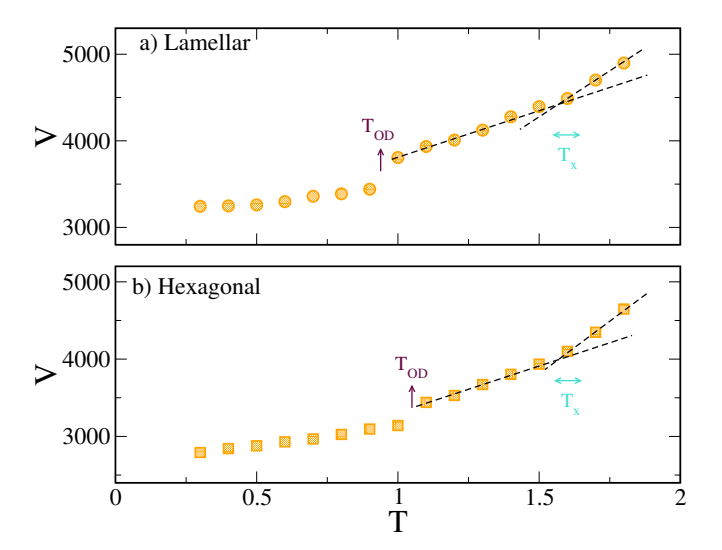


FIG. 1. Equilibrated volume at different temperatures for both analyzed systems. (a) In the lamellar system, an order-disorder transition (T_{OD}) close to 0.95 is observed, indicated with a brown arrow. (b) For the hexagonal system, T_{OD} is identified around 1.05. Additionally, in both graphs, a double arrow and a dashed black line are included to highlight the change in slope within the high-temperature region, denoted as T_x .

tures below T_x , the structural connections between particles become evident, permitting the observation of such wormlike micelles.

These three regimes have been structurally characterized in a previous work³⁹. In the following sections of this study, we will thoroughly analyze various dynamic aspects of the system. This comprehensive approach will enable us to delve into the underlying causes behind the observed changes, offering a more complete perspective on the dynamics of the system under study. The focus of this work is on the dynamic characterization of each system individually, rather than on a comparative analysis between the different systems. This is an interesting avenue that we plan to explore in future research.

Moving forward, we analyze the dynamic behavior of the systems at the various temperatures examined. Initially, we consider the mean square displacements (MSD) of the particles, defined as:

$$\langle r^2(t)\rangle = \frac{1}{N} \sum_{i=1}^{N} |\mathbf{r}_i(t) - \mathbf{r}_i(0)|^2$$
 (2)

where N is the total number of particles considered in the calculation, $\mathbf{r}_i(t)$ is the position of particle i at time t, and $\mathbf{r}_i(0)$ is the initial position at time t = 0.

Figure 3 shows the behavior of this magnitude for the hexagonal-forming system at different temperatures. In Figure 3-a, all particles of the system are considered, while Figure 3-b focuses solely on the minority particles (type B).

micelation/clusterization mesophase formation T<T_{OD} $T_{OD} < T < T_X$ $T>T_X$ Temperature

FIG. 2. Visualization of the structural changes in the hexagonal system across temperature variations, highlighting the spatial arrangement of particles in three distinct thermal regions. On the left, for $T < T_{OD}$, the ordered and hexagonal structure is shown with grey spheres representing the majority particles (type A) and blue isosurfaces representing the minority particles (type B), indicating a clear organization in the mesophase. In the center, for $T_{OD} < T < T_x$, an intermediate phase of micellization with visible wormlike clusters of minority particles is observed. On the right, for $T > T_x$, the system adopts an isotropic state without micellization and a homogeneous distribution of particles.

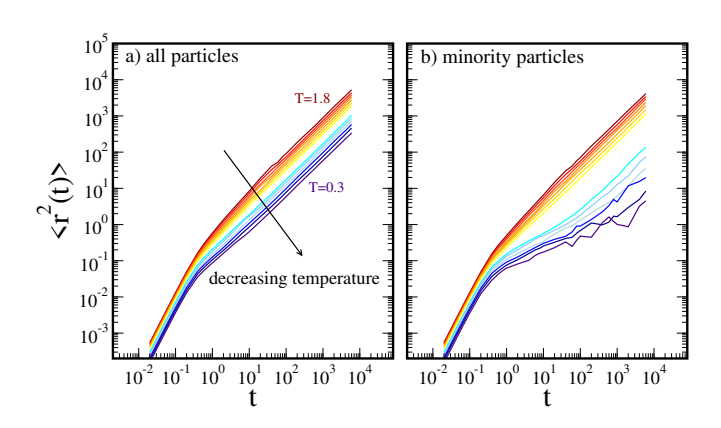


FIG. 3. Mean square displacement of the hexagonal system at different temperatures: (a) shows the displacement for all the particles of the system, while (b) details the specific displacement of the minority particles. The temperature values corresponding to the curves are as follows: 1.8, 1.7, 1.6, 1.5, 1.4, 1.3, 1.2, 1.1, 1.0, 0.9, 0.8, 0.7, 0.6, 0.5, 0.4, and 0.3. The color scales indicate the regimes relative to the order-disorder transitio: shades of blue represent temperatures below T_{OD} (within the mesophase), while shades of red correspond to temperatures above T_{OD} (in the isotropic phase).

On the other hand, Figure 4 performs the same analysis but for the lamellar-forming system.

It is observed in both systems that throughout the entire range of temperatures examined, including those within the ordered phase, the overall dynamic behavior of the system is remarkably active, exhibiting high mobility. However, for the hexagonal system, the behavior of the minority particles aligns with this scenario of high activ-

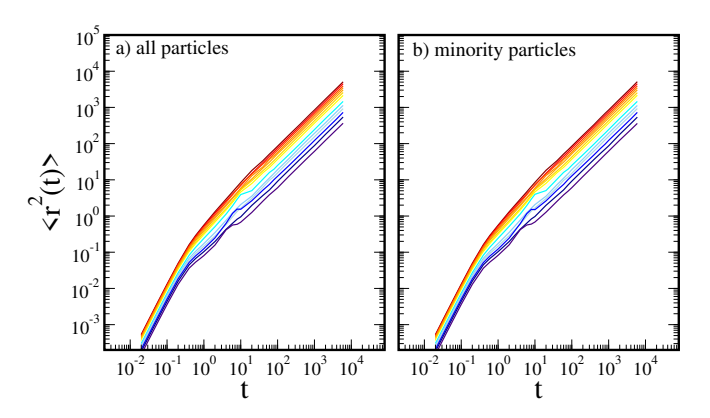


FIG. 4. Mean square displacement of the lamellar system at different temperatures: (a) shows the displacement for all the particles of the system, while in (b) the specific displacement of the minority particles is detailed. Refer to Figure 3 for the detailed temperature values analyzed in this study. The color scale indicates regimes relative to T_{OD} : blue shades for below T_{OD} (mesophase) and red shades for above T_{OD} (isotropic

ity only at elevated temperatures. Below T_{OD} , these particles start to notably diverge from the general behavior, exhibiting significantly slower dynamics. In this regime, a subdiffusive behavior of the minority particles becomes apparent. This pronounced slowdown of the minority particles in the hexagonal system can be attributed to the extreme degree of confinement experienced by these particles. The ordering in the hexagonal phase occurs at the scale of a single particle diameter, unlike in other systems where the structures, such as cylinders or lamellae, involve multiple particles of the same type. This unique aspect of the KM model leads to a significant confinement for the minority particles. This particular configuration, where minority particles lack bulk neighbors of the same type, is likely the key reason behind the observed subdiffusive behavior, making this slowdown specific to this system and not easily generalizable to other microphase formers.

Complementing this analysis, we have calculated the diffusion coefficients using the Einstein relation:

$$D = \frac{1}{6t} \lim_{t \to \infty} \langle r^2(t) \rangle,$$

which allows us to determine the diffusion coefficients at various temperatures and calculate the activation energies associated with the mobility of the particles in the different phases. The activation energy for diffusion is obtained by analyzing the temperature dependence of the diffusion coefficient through an Arrhenius plot, where the logarithm of the diffusion coefficient is plotted against the inverse of the temperature. The slope of the linear regression in each temperature region corresponds to the activation energy, providing insights into the energy barriers that govern particle mobility in the respective region.

In Figures 5-a and 5-b, the D(T) values for the different systems are presented as a function of the inverse temperature. The order-disorder transition is clearly reflected in this magnitude, with a noticeable change in the activation energies depending on whether the system is in an ordered state or not. For both systems, a similar behavior is observed when analyzing the global diffusion: the structuring of the system tends to facilitate dynamics by reducing the activation energy for diffusion. This is evident from the activation energy values indicated in the figures. This decrease in activation energy when the mesophase forms below T_{OD} can be explained by the interaction potential between different types of particles and the structural changes involved in the transition. When these systems become structured, there is an increase in contact between particles of the same type (AA and BB)³⁹. Since the interactions between particles of the same type $(\epsilon_{AA}$ and $\epsilon_{BB})$ are weaker compared to those between different types (ϵ_{AB}) , this structuring reduces the energy barriers for diffusion.

A notable aspect in the hexagonal system, when considering only the minority particles, is that although the change at T_{OD} is evident, the activation energy do not show a marked change at this characteristic temperature, unlike the case with indistinguishable particles. This suggests that the mobility mechanism for these minority particles remains consistent below the transition, which could be expected given the local structuring these particles exhibit, similar to the mesophase. On the other hand, around T_x , where a slope change might be anticipated due to clustering, no appreciable changes in activation energies are observed.

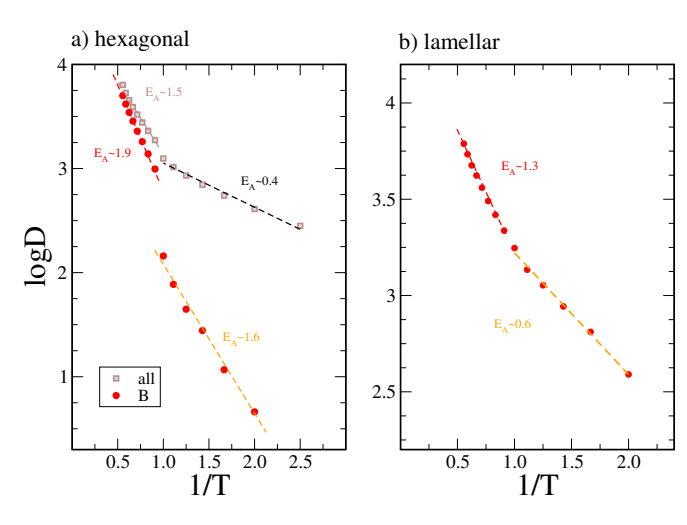


FIG. 5. Diffusion coefficients as a function of the inverse temperature for both analyzed systems: (a) hexagonal system and (b) lamellar system. The calculation was performed by distinguishing particles by type (B) and considering them as indistinguishable (all). The activation energies for each temperature region were calculated and are indicated in each case.

Following a similar line to the study of mobility, we

have also investigated the incoherent intermediate scattering function, another typical function used in the study of structural relaxation in Molecular Dynamics simulations. This function, denoted as $F_s(\mathbf{k},t)$, is defined as:

$$F_s(k,t) = \frac{1}{N} \sum_{i=1}^{N} \exp(-i\mathbf{k} \cdot \mathbf{r}_i(t)), \qquad (3)$$

which represents the average of the exponential of the dot product between the wave vector \mathbf{k} and the position vector of each particle i at time t.

We evaluate $F_s(\mathbf{k},t)$ at the wave vector $\mathbf{k}=4.2$, corresponding to the first peak in the g(r). Figure 6 shows the behavior of this function for the hexagonal-forming system at different temperatures. The graph on the left includes all particles, while the graph on the right focuses exclusively on type B particles. In general terms, the function shows a rapid decay for most of the temperatures analyzed; however, at the lower temperatures, the decay for the minority particles is notably slower compared to the overall behavior. The same comparison is presented for the lamellar-forming system in Figure 7, where it is observed that the behavior of type B particles largely overlaps with the overall behavior, which was expected given the nature of the system.

From the analysis of how this function decays, it is possible to calculate the structural relaxation time, τ , for each temperature, defined as $F_s(\mathbf{k}, \tau) = e^{-1}$.

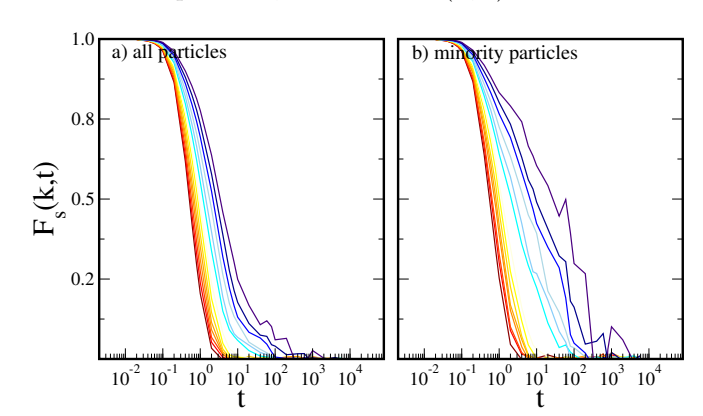


FIG. 6. The incoherent intermediate scattering function was analyzed at different temperatures in the hexagonal system. For case (a), all particles of the system are considered, while in case (b) it focuses exclusively on the minority particles. Refer to Figure 3 for the detailed temperature values analyzed in this study. The color scale indicates regimes relative to T_{OD} : blue shades for below T_{OD} (mesophase) and red shades for above T_{OD} (isotropic phase).

In Figure 8, we illustrate the relaxation times as a function of the inverse temperature for the hexagonal-forming system, where, similar to the previous analysis, we can calculate the activation energies for relaxation. Similar to the diffusion coefficients, a notable change in the structural relaxation times around T_{OD} is observed, making

FIG. 7. The incoherent intermediate scattering function was analyzed at different temperatures in the lamellar system. For case (a), all particles of the system are considered, while in case (b) it focuses exclusively on the minority particles. Refer to Figure 3 for the detailed temperature values analyzed in this study. The color scale indicates regimes relative to T_{OD} : blue shades for below T_{OD} (mesophase) and red shades for above T_{OD} (isotropic phase).

this dynamic parameter useful for capturing the ordering transition. In the specific case of considering all particles as indistinguishable, a significant change is noted at T_{OD} , with the system transitioning from a higher activation energy for relaxation in the isotropic phase to a lower energy in the mesophase. This change is attributed to the increased mutual contact among the same particle types as the mesophase forms, a phenomenon we have previously mentioned.

Focusing specifically on type B particles in the hexagonal system, the change observed at T_{OD} is more abrupt, particularly in terms of the sharp changes in τ values at this temperature. However, the variations in activation energy are not as pronounced, showing similar slopes, much like the behavior observed for the diffusion coefficients. In the high-temperature region, represented in the inset of Figure 8, no appreciable changes in the activation energy are observed when considering all particles in the system within this region. However, for the minority particles, an anomaly around T_x is noted, which seems to reflect a change in the slopes, as indicated by the dashed lines. From this analysis, it is inferred that the activation energies decrease for temperatures below T_x in the subsystem of minority particles in the hexagonal system. This behavior is attributed to significant clustering below T_x , where this regime, observed visually as worm-like or elongated clusters, clearly resembles the mesophase. Consequently, the activation energy for the structural relaxation of the minority particles is similar to that in the mesophase.

In the lamellar system, as shown in Figure 9, a significant change in structural relaxation times is observed around T_{OD} , similar to what is seen in the hexagonal system. This transition is clearly reflected in the change in activation energies. The values of this quantity above

 T_{OD} are comparable to those of the hexagonal system. This similarity can be explained by the presence of wormlike structures in both systems at high temperatures. However, once the lamellar mesophase forms, the activation energy decreases more significantly compared to the hexagonal system, with a reduction by a factor of approximately 4 in the lamellar system versus a factor of approximately 2 in the hexagonal system. This greater decrease can be attributed to the lower confinement in the lamellae, where there are entire planes that allow particles of the same type to reorganize, in contrast to the more restricted environment of the hexagonal structure. In the high-temperature region, as shown in the inset of Figure 9, no changes in behavior are observed around T_x . Due to the high proportion of particles, with no minority particles in this system, the structural changes at T_x do not significantly affect the relaxation mechanism.

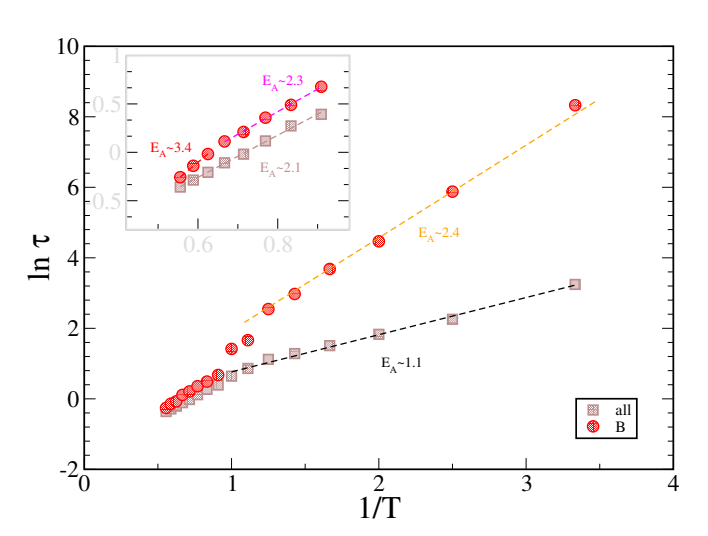


FIG. 8. Structural relaxation times as a function of the inverse temperature for the hexagonal system are graphically represented, where the red dots correspond to the minority particles, while the brown squares represent all particles in the system. In the inset, the behavior in the high-temperature regions is magnified, allowing a detailed observation of the differences in relaxation behavior between the minority particles and the total set of particles. The activation energies for each temperature region were calculated and are indicated in each case.

In the following section, we will implement a function that allows us to quantify a specific dynamic correlation⁴¹. This function assesses how the movement of a particle is, or is not, influenced by the particles in its immediate surroundings. To achieve this, we calculate dynamic entities called *strings*, which represent a type of correlated movement where particles successively replace each other in their trajectories. The identification of these coordinated movements, or *string* movements, allows us to detect the occurrence of such dynamic events at different moments in time. One commonly used method to identify a *string* and quantify the

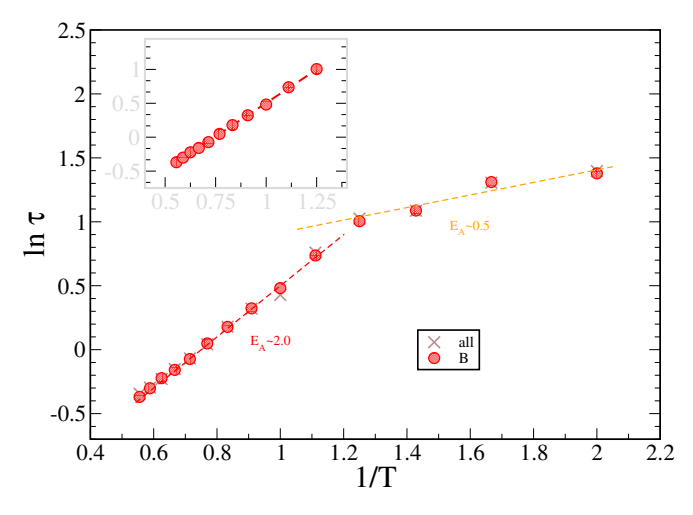


FIG. 9. The analysis of structural relaxation times as a function of inverse temperature was similarly conducted for the lamellar system. The red dots and brown squares represent, respectively, the minority particles and all the particles in the system, as previously described for the hexagonal system. The specific behavior of the lamellar system, especially in the high-temperature regions, is detailed in the corresponding inset. The activation energies for each temperature region were calculated and are indicated in each case.

number of particles involved in these chain movements involves defining a string by connecting two particles i and j if they meet the following minimum condition:

$$\min\left\{\Delta r_{ij}(t), \Delta r_{ji}(t)\right\} < 0.35,\tag{4}$$

where $\Delta r_{ij}(t) = ||r_i(t) - r_j(t_0)||$ represents the distance between the temporal position of particle i at time t, $r_i(t)$, and the initial position of particle j at time t_0 , $r_i(t_0)$. This analysis can also be restricted to particles of the same type, ensuring that i and j correspond to a single particle species. This minimum condition indicates that one of the particles has moved, and another particle has occupied its previous position. The value of 0.35 is the maximum distance threshold we impose to define the replacement of the position of one particle by another. This methodology has been widely applied in the study of cooperative rearranging regions (CRRs), a phenomenon commonly observed in glass formers 41,42 . Based on this definition, we calculate various statistical parameters, such as the average size of the detected strings, L(t), and the maximum string size at a given temperature, $L^*(T)$. In our case, we also count individual particles as contributing to a string of unit size.

The temporal behavior of this dynamic parameter for different temperatures is shown in Figure 10 for the hexagonal-forming system and Figure 11 for the lamellar-forming system. This function presents unitary values at very short times, that is, no *strings* are recorded, then the function increases until reaching a maximum, at a time within the same order of magnitude as the structural relaxation. For longer times, the curves decline because the

string type mobility mechanism becomes very infrequent. Another noteworthy fact is that considering all particles versus only the minority ones leads to a significant difference in the case of the hexagonal system, a phenomenon that is less pronounced in the lamellar system.

It is worth noting that the average string sizes are relatively small, indicating that most particles exhibit movement independent of this mechanism, in contrast to what occurs in glass formers as they approach the glass transition temperature. One might also expect a more abrupt increase in string sizes in mesophase-forming systems that exhibit clustering, particularly when the dynamics are strongly conditioned and significantly slowdown, as seen in SALR systems³⁰. Although this is not the case in the present model, as discussed below, this parameter can still be useful for distinguishing whether the system is above or below T_{OD} .

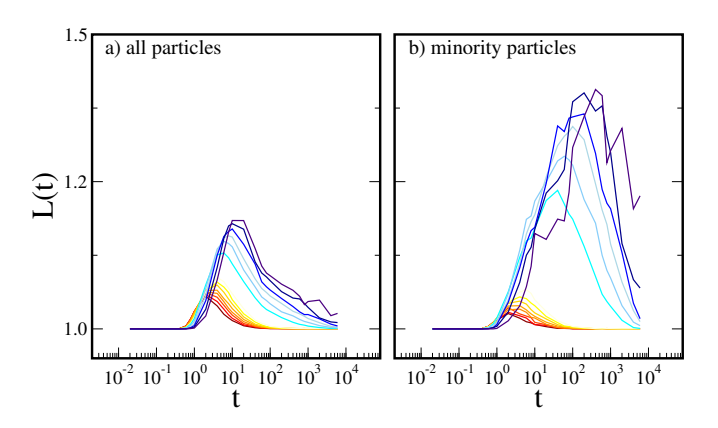


FIG. 10. Average size of strings in the hexagonal system as a function of time at various temperatures. For case (a), all particles of the system are considered, while in case (b) it focuses exclusively on the minority particles. Refer to Figure 3 for the detailed temperature values analyzed in this study. The color scale indicates regimes relative to T_{OD} : blue shades for below T_{OD} (mesophase) and red shades for above T_{OD} (isotropic phase).

In Figure 12, the maximum size of strings for each temperature $(L^*(T))$ is shown. A notable change at the ordering transition is observed for both systems. This suggests, in correlation with the decrease in activation energies for diffusion associated with ordering, that the formation of the mesophase—characterized by greater contact among particles of the same type—encourages more coordinated movement.

In line with the analysis of the L(t) curves, the lamellar-forming system does not show significant differences when comparing all particles with the minority ones. However, in the hexagonal-forming system, a notable difference is observed below T_{OD} . Furthermore, in the isotropic phase, considering exclusively one type of particle results in a lower value of $L^*(T)$ compared to analyses that include all particles. Interestingly, this trend reverses below T_{OD} .

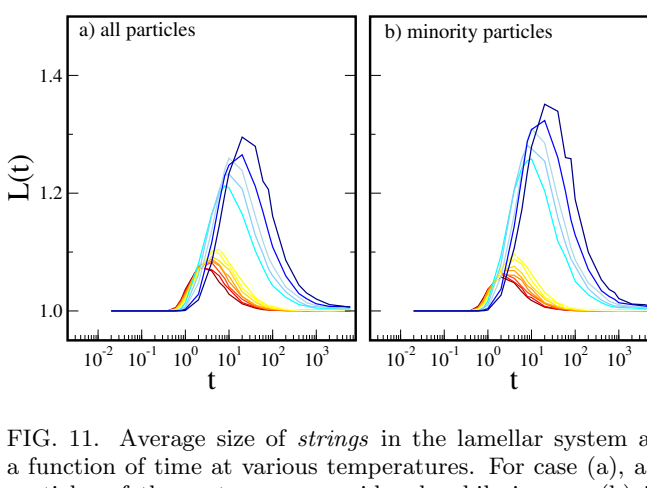


FIG. 11. Average size of strings in the lamellar system as a function of time at various temperatures. For case (a), all particles of the system are considered, while in case (b) it focuses exclusively on the minority particles. Refer to Figure 3 for the detailed temperature values analyzed in this study. The color scale indicates regimes relative to T_{OD} : blue shades for below T_{OD} (mesophase) and red shades for above T_{OD} (isotropic phase).

It is important to highlight that, although the degree of string-type mobility is generally low, it is sufficiently significant to mark the transition. This could be considered a valuable dynamic parameter to document this type of change. It is interesting to note that no defined change is observed at T_x within this dynamic framework analyzed; therefore, the changes observed at this temperature in dynamic behavior are not related to this specific mobility mechanism. In other words, the observed clustering does not seem to trigger a dynamic mechanism of the string type or replacement.

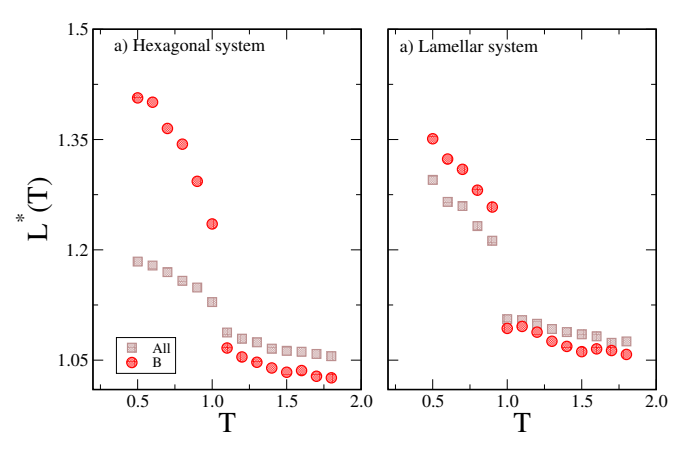


FIG. 12. Maximum string sizes for different temperatures in two systems: (a) hexagonal and (b) lamellar. Red dots represent the minority particles, while brown squares denote all particles within the system. Although a distinct change is observed at T_{OD} , no significant behavioral shift is evident at T_{T} .

Finally, with the purpose of analyzing the correlated

movement between particles and determining if the dynamic mechanism can be characterized more effectively at different temperatures, we proceed to calculate the Pearson correlation coefficient (k_{ij}) to examine the dynamic correlations between particles within a set of trajectories in an isoconfigurational ensemble (ICE)⁴³.

The isoconfigurational ensemble (ICE) is a method where the dynamics of a system are studied starting from a single initial configuration. Multiple realizations or trajectories are generated using molecular dynamics simulations, each with different initial velocities randomly assigned according to the same statistical distribution. This approach enables the investigation of the intricate relationship between dynamic behavior and structural properties in complex systems, such as glasses. By examining how different velocity initializations influence the system's evolution, ICE helps to uncover underlying patterns and mechanisms that govern the material's behavior 44–50.

The use of k_{ij} allows investigating the dynamic interaction between pairs of particles separated by a distance r_{ij} . This coefficient is defined as follows:

$$k_{ij}(r) = \frac{1}{S_i S_j} \sum_{w=1}^{N_{IC}} (\mathbf{r}_i(w, t) - \langle \Delta \mathbf{r}_i \rangle_{IC}) \cdot (\mathbf{r}_j(w, t) - \langle \Delta \mathbf{r}_j \rangle_{IC}),$$
(5)

where N_{IC} represents the total number of trajectories in the ICE, and S_i , S_j are the standard deviations of the displacements of particles i and j, respectively, within the set of trajectories of the ensemble.

The coefficient $|k_{ij}(t)|$ can vary between 0 and 1, serving as a measure of how the displacement of one particle i is related to that of another j. A correlation greater than zero suggests that both particles tend to move similarly, whether in large or small magnitude, or that significant movement of one can induce lesser movement in the other^{44,51}. Conversely, a low coefficient value indicates that the relative movement of the particles is fundamentally independent.

Moreover, in order to establish an individualized parameter for each particle, we have calculated K_i considering correlation with all neighboring particles 49,52,53 . This is achieved by averaging the values of $|k_{ij}|$ that meet the condition $r_{ij}(t=0) = |r_i(0) - r_j(0)| < r_{\rm nbr}$, where $r_{\rm nbr}$ denotes the distance of first neighbors, determined by the minimum in the radial distribution function. This approach allows us to differentiate dynamics according to the specific type of particles involved in the relation i with j. In our analysis, we distinguish between the interactions of type B particles with the rest of the system (B-All) and exclusively between type B particles (B-B).

In Figure 13, the behavior of K(t), which represents the average of K_i , for the hexagonal-forming system is illustrated. A similar analysis is conducted for the lamellar-forming system, as shown in Figure 14. It is observed that, in all cases, the correlation between particles is zero at short times. Subsequently, the correlation increases until reaching a maximum, approximately at

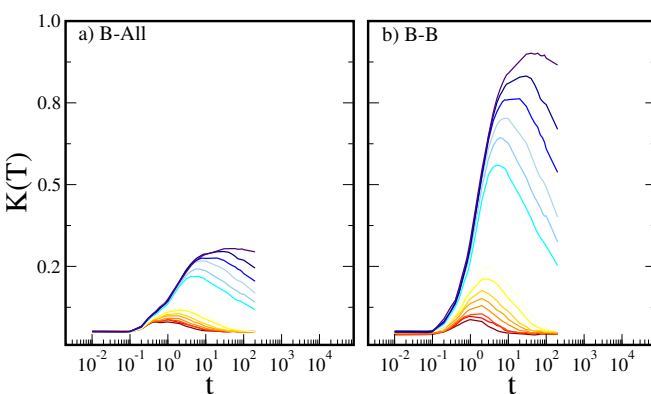


FIG. 13. Values of Pearson's dynamic correlation magnitude for the hexagonal system. For case (a), all particles of the system are considered, while in case (b) it focuses exclusively on the minority particles. For the analyzed temperature values, refer to Figure 3, where they are detailed. The color scale indicates regimes relative to T_{OD} : blue shades for below T_{OD} and red shades for above T_{OD} .

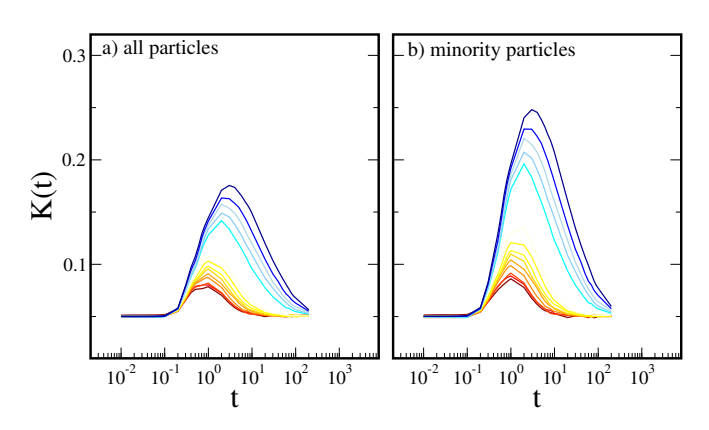


FIG. 14. Values of Pearson's dynamic correlation magnitude for the lamellar system. For case (a), all particles of the system are considered, while in case (b) it focuses exclusively on the minority particles. For the analyzed temperature values, refer to Figure 3, where they are detailed. The color scale indicates regimes relative to T_{OD} : blue shades for mesophase and red shades for isotropic phase.

Next, we proceeded to calculate the maximum values reached by K(t) for each temperature. The results are illustrated in Figures 15 for the hexagonal- and 16 for the lamellar-forming system. A noticeable and abrupt

change in this magnitude around the phase transition in both systems is observed. This change is particularly pronounced in the hexagonal system when exclusively analyzing the minority particles. Interestingly, in this same system, a change in behavior at T_x is evidenced, with an increase in slope below this temperature, suggesting a particularly relevant dynamics at this point. Notably, the change in slope is quite sharp. Although a similar pattern is observed in the lamellar system, the change is significantly smoother.

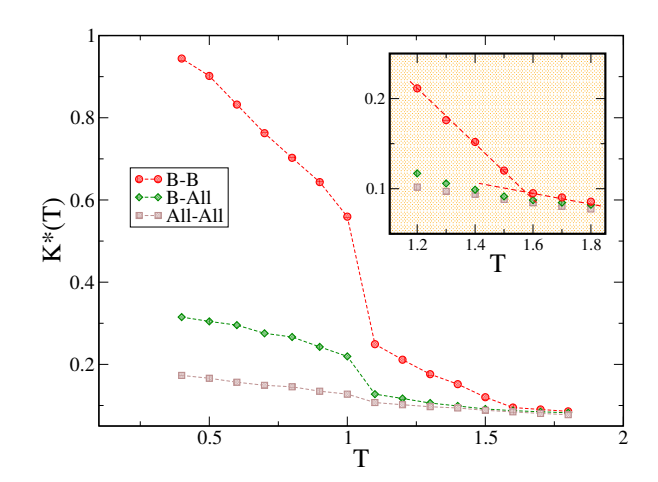


FIG. 15. Maximum values of K(t) for various temperatures in the hexagonal system, highlighting significant changes in dynamics near the phase transition, particularly pronounced in minority particles. The inset displays the region around T^* , with lines indicating the observed crossover behavior at this temperature.

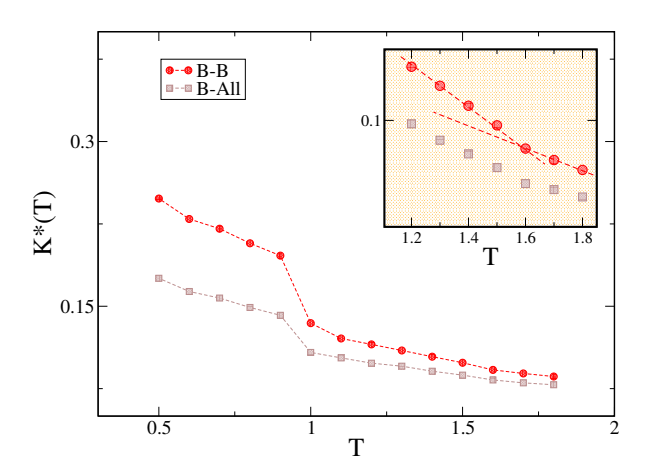


FIG. 16. Maximum values of K(t) for various temperatures in the lamellar system, illustrating subtle dynamic changes near the phase transition. Unlike in the hexagonal system, changes in the lamellar system are less pronounced, particularly in minority particles. The inset shows the region around T^* , with lines depicting the more gradual crossover behavior observed at this temperature.

This is the author's peer reviewed, accepted manuscript. However, the online version of record will be different from this version once it has been copyedited and typeset

This latter phenomenon can be related to the processes occurring around T_x , where the formation of clusters becomes evident. At this temperature, particles of the same type begin to exhibit more correlated movements among themselves. Unlike the string type displacements described earlier, this relative and correlated movement is characterized by being more coordinated, implying a dynamic interaction that does not necessarily translate into a direct change of position between particles, but rather reflects a greater dynamic connection in the environment of the particles. Similar to observations in systems with short-range attraction and long-range repulsion interactions, where clusters are more stable than the homogeneous liquid across a broad range of densities and temperatures^{22,54–59}, the dynamic clustering observed here suggests a significant structural organization. This clustering process does not represent a conventional phase transition but rather a morphological change within the disordered microphase regime, and its definition involves a degree of arbitrariness^{22,54}. The formation of clusters in the isotropic phase thus emerges as a critical precursor that influences both the structure and dynamics of the system, highlighting the complex phenomenology associated with this clustering regime. As shown by Santos et al., the presence of these dynamic clusters alters the system's thermodynamic properties significantly, mirroring the changes observed in our model at T_x^{40} .

IV. CONCLUSION

In this study, through molecular dynamics simulations using a model of spheres with isotropic interactions, we conducted a detailed investigation of the dynamic behavior of particles in systems that form hexagonal and lamellar mesophases.

We identified three distinct dynamic regimes based on temperature, which correspond to the three structural regimes characterized in our previous work: ordered microphases at low temperature, a disordered phase at high temperature, and a disordered cluster regime in between.

Through the dynamic analysis carried out in this work, where we examined the activation energies for structural relaxation and diffusion, as well as the dynamic correlations among particles, we were able to explore the changes in mobility mechanisms across the different observed regimes. This analysis not only enabled us to characterize the order-disorder transition at a specific temperature (T_{OD}) , but it also provided insights into the crossover behavior at the temperature where clustering becomes noticeable (T_x) . These studies contribute to a deeper understanding of mesophase formation.

ACKNOWLEDGMENTS

This work was supported by Agencia I+D+I (PICT-2020-SERIEA-00698) and CONICET (PIBAA-0698).

We used Mendieta Cluster from CCAD-UNC which is part of SNCAD-MinCyT, Argentina. MVUW acknowledges the doctoral scholarship from CONICET, Argentina.

- ¹G. M. Whitesides and M. Boncheva, Science **295**, 2418 (2002).
- ²T. Aida, E. W. Meijer, and S. I. Stupp, Nature **476**, 28 (2012).
- ³A. W. Adamson, A. P. Gast, et al., Physical chemistry of surfaces, Vol. 150 (Interscience publishers New York, 1967).
- ⁴F. S. Bates and G. H. Fredrickson, Annual review of physical chemistry **41**, 525 (1990).
- 5 G. M. White sides and M. Boncheva, Proceedings of the National Academy of Sciences $\bf 99,\,4769$ (2002).
- ⁶J.-M. Lehn, Supramolecular chemistry (VCH, 1993).
- ⁷Y. Min, M. Akbulut, K. Kristiansen, Y. Golan, and J. Israelachvili, Nature materials 7, 527 (2008).
- ⁸G. M. Grason, Physics Reports **433**, 1 (2006).
- ⁹S. C. Glotzer and M. J. Solomon, AIChE Journal **50**, 2978 (2004).
- ¹⁰S. C. Glotzer and M. J. Solomon, Nature materials **6**, 557 (2007).
- ¹¹C. R. Harkless, M. A. Singh, S. E. Nagler, G. B. Stephenson, and J. L. Jordan-Sweet, Phys. Rev. Lett. **64**, 2285 (1990).
- ¹²B. Stuehn, A. Vilesov, and H. G. Zachmann, Macromolecules 27, 3560 (1994).
- ¹³A. Arora, J. Qin, D. C. Morse, K. T. Delaney, G. H. Fredrickson, F. S. Bates, and K. D. Dorfman, Macromolecules 49, 4675 (2016).
- ¹⁴W.-S. Xu *et al.*, Journal of Physical Chemistry B **122**, 3549 (2018).
- 15R. G. Larson, The Journal of Chemical Physics **96**, 7904 (1992).
- ¹⁶A. P. Santos and A. Z. Panagiotopoulos, The Journal of Chemical Physics **144**, 044709 (2016).
- ¹⁷R. D. Groot and T. J. Madden, The Journal of Chemical Physics 108, 8713 (1998).
- ¹⁸M. Müller and J. J. de Pablo, Annual Review of Materials Research 43, 1 (2013).
- ¹⁹R. D. Groot, T. J. Madden, and D. J. Tildesley, The Journal of Chemical Physics **110**, 9739 (1999).
- ²⁰M. W. Matsen, G. H. Griffiths, R. A. Wickham, and O. N. Vassiliev, The Journal of Chemical Physics 124 (2006).
- $^{21}\mathrm{G.}$ Srinivas, D. E. Discher, and M. L. Klein, Nature materials 3, 638 (2004).
- ²²Y. Zhuang and P. Charbonneau, The Journal of Physical Chemistry B 120, 7775 (2016).
- ²³A. Kumar and V. Molinero, The Journal of Physical Chemistry Letters 8, 5053 (2017).
- ²⁴K. Binder, Monte Carlo and Molecular Dynamics Simulations in Polymer Science (Oxford University Press, 1995).
- ²⁵A. Ciach and A. Góźdź, Physical Review Letters 93, 055701 (2004).
- ²⁶P. H. Nelson, G. C. Rutledge, and T. A. Hatton, The Journal of Chemical Physics **107**, 10777 (1997).
- ²⁷A. Archer and N. Wilding, Nature **437**, 363 (2004).
- ²⁸F. Sciortino, P. Tartaglia, and E. Zaccarelli, Physical Review Letters 110, 238301 (2004).
- ²⁹E. Zaccarelli, Journal of Physics: Condensed Matter 17, S3223 (2005).
- ³⁰M. Zheng and P. Charbonneau, The Journal of Chemical Physics 154, 244506 (2021).
- ³¹J. Pekalski, A. Ciach, and N. G. Almarza, The Journal of Chemical Physics 138, 144903 (2013).
- ³²S. J. Marrink and D. P. Tieleman, Chemical Society Reviews 42, 6801 (2013).
- ³³A. Kumar, A. H. Nguyen, R. Okumu, T. D. Shepherd, and V. Molinero, Journal of the American Chemical Society 140, 16071 (2018).
- ³⁴A. Kumar and V. Molinero, The Journal of Physical Chemistry B 122, 4758 (2018).
- ³⁵A. Kumar and V. Molinero, The Journal of Physical Chemistry Letters 9, 5692 (2018).

This is the author's peer reviewed, accepted manuscript. However, the online version of record will be different from this version once it has been copyedited and typeset

PLEASE CITE THIS ARTICLE AS DOI: 10.1063/5.0224154

- ³⁶A. J. Mukhtyar and F. A. Escobedo, Macromolecules 51, 9769 (2018).
- ³⁷S. Plimpton, Journal of Computational Physics **117**, 1 (1995).
- ³⁸R. S. DeFever, C. Targonski, S. W. Hall, M. C. Smith, and S. Sarupria, Chemical science 10, 7503 (2019).
- ³⁹M. V. U. Wassermann, E. R. Soulé, and C. Balbuena, Journal of Molecular Liquids 411, 125713 (2024).
- ⁴⁰ A. P. Santos, J. Pekalski, and A. Z. Panagiotopoulos, Soft Matter 13, 8055 (2017).
- ⁴¹C. Donati, J. F. Douglas, W. Kob, S. J. Plimpton, P. H. Poole, and S. C. Glotzer, Phys. Rev. Lett. **80**, 2338 (1998).
- ⁴²M. Aichele, Y. Gebremichael, F. W. Starr, J. Baschnagel, and S. C. Glotzer, The Journal of Chemical Physics 119, 5290 (2003).
- ⁴³ A. Widmer-Cooper, P. Harrowell, and H. Fynewever, Phys. Rev. Lett. 93, 135701 (2004).
- ⁴⁴A. Widmer-Cooper and P. Harrowell, The Journal of Chemical Physics **126**, 154503 (2007).
- ⁴⁵ A. Widmer-Cooper, H. Perry, P. Harrowell, and D. R. Reichman, Nature Physics 4, 711 (2008).
- ⁴⁶ A. Widmer-Cooper, H. Perry, P. Harrowell, and D. R. Reichman, The Journal of Chemical Physics 131, 194508 (2009).
- ⁴⁷C. Balbuena, M. A. Frechero, and R. A. Montani, Solid State Ionics 262, 493 (2014).

- ⁴⁸J. Qin and S. T. Milner, Macromolecules **47**, 6077 (2014).
- ⁴⁹C. Balbuena, M. M. Gianetti, and E. R. Soulé, The Journal of Chemical Physics **150**, 234508 (2019).
- ⁵⁰A. R. Verde, L. M. Alarcón, and G. A. Appignanesi, The Journal of Chemical Physics 158, 114502 (2023).
- ⁵¹C. Balbuena, M. M. Gianetti, and E. R. Soulé, The Journal of Chemical Physics **149**, 094506 (2018).
- ⁵²C. Balbuena and E. R. Soulé, Journal of Physics: Condensed Matter **32**, 045401 (2019).
- ⁵³C. Balbuena, M. Mariel Gianetti, and E. Rodolfo Soulé, Soft Matter 17, 3503 (2021).
- ⁵⁴Y. Zhuang, K. Zhang, and P. Charbonneau, Phys. Rev. Lett. 116, 098301 (2016).
- ⁵⁵Y. Zhuang and P. Charbonneau, The Journal of Chemical Physics 147, 091102 (2017).
- ⁵⁶M. Tarzia and A. Coniglio, Phys. Rev. E **75**, 011410 (2007).
- ⁵⁷J.-M. Bomont, J.-L. Bretonnet, D. Costa, and J.-P. Hansen, The Journal of Chemical Physics 137, 011101 (2012).
- ⁵⁸ J.-M. Bomont, D. Costa, and J.-L. Bretonnet, Phys. Chem. Chem. Phys. **19**, 15247 (2017).
- ⁵⁹Y. Hu and P. Charbonneau, Soft Matter, 4101 (2018).